Aerospace Science and Technology 110 (2021) 106445

Contents lists available at ScienceDirect

Aerospace Science and Technology

www.elsevier.com/locate/aescte

Broadband modified-circle-shape patch antenna with H-aperture feeding for a passive radar array ☆

J. Rosado-Sanz *, M.P. Jarabo-Amores *, D. Mata-Moya, P.J. Gómez-del-Hoyo, N. Del-Rey-Maestre

Signal Theory and Communications Department, University of Alcalá, Alcalá de Henares (Madrid), Spain

ARTICLE INFO

Article history:
Received 2 August 2019
Received in revised form 18 August 2020
Accepted 13 December 2020
Available online 12 January 2021
Communicated by Amit Sanyal

Keywords:
Patch antenna
Broadband
Circle-shape
H-aperture
NULA
Passive radar

ABSTRACT

In this paper, the design of a broadband modified-circle-shape patch antenna with H-aperture feeding is presented, to be used as single radiating element in the array of the surveillance channel of an UHF passive radar. Different techniques are proposed to achieve a relative bandwidth of more than 30%, and challenging radiation pattern characteristics for the defined application. The achievement of these requirements is proved through measurements in anechoic chamber. A NULA is designed using optimization techniques and considering coupling effects between elements. The NULA was integrated in IDEPAR, the passive radar demonstrator developed in the University of Alcalá, and validated through measurement campaigns. Results prove a significant improvement of the passive radar target detection and bearing estimation capabilities.

1. Introduction

Passive Radars (PRs) are emerging surveillance technologies that exploit transmitters belonging to other communication system (commercial broadcasting, radio communications or radar and radio-navigation systems), which are called Illuminators of Opportunity (IoO), instead a dedicated one [1,2]. Target detection and parameters estimation are based on the radar echoes generated by objects illuminated by the IoOs.

Due to the lack of control of the IoO, a reference channel is used to capture the direct IoO signal; the surveillance one acquires target echoes in the coverage area. In Fig. 1, the system geometry and the basic components of a bistatic PR are shown: (a) L is the IoO-to-radar distance (base-line); (b) $\sigma_{bis,i}$ is the target Bistatic Radar Cross Section (BRCS), which models the power that is scattered from the target towards the PR receiver, when it is illuminated by the IoO; (c) R_{Ri} and R_{Ti} are the radar-to-target and target-to-IoO distances, respectively; (d) β_i is the bistatic angle.

PR target detection is usually based on the correlation of the surveillance signal ($\tilde{s}_{surv}[n]$) with Doppler shifted copies of the reference one ($\tilde{s}_{ref}[n]$), to generate the Cross-Ambiguity Function (CAF) (1).

$$S^{CAF}[m,p] = \sum_{n=0}^{N-1} \tilde{s}^{*}_{ref}[n-m] \cdot \tilde{s}_{surv}[n] \cdot \exp^{-j2\pi \frac{p}{N} n} \tag{1}$$

$N = T_{int} \cdot f_s$, is the number of samples, being T_{int} (s) the integration time, which defines the duration of the Coherent Processing Interval (CPI), and f_s (Hz) the sampling frequency; m is the time bin associated with a delay $\tau_m = m/f_s$, and p is the Doppler-shift corresponding to $f_{dop} = f_s\,(p/N)$. Targets delay and Doppler shifts are estimated from the maxima of the CAF amplitude generated per each CPI.

The absence of a dedicated and controlled transmitter provides some advantages to PRs against active radars, as reduced deployment, maintenance and update costs, absence of electromagnetic compatibility issues, and low probability of interception, that have awaken research interest for different applications, such as air traffic control [3–5] or protection of critical infrastructures, especially against drones' attacks [6,7]. But, the use of waveforms not designed for detection purposes gives rise to the necessity of designing complex signal processing techniques, and antenna systems fulfilling radar detection requirements: FM circular array of dipoles [8,4]; circular array of biquad antennas to improve DoA at UHF frequencies [9]; combination of array antennas to cover VHF

☆ This work was supported by the Spanish "Ministerio de Ciencia, Innovación y Universidades" under Project RTI2018-101979-B-I00; "Junta de Comunidades de Castilla-La Mancha" under Project SBPLY/19/180501/000350; and "Comunidad de Madrid" under Project CM/JIN/2019-027.

* Corresponding authors.
E-mail addresses: javier.rosado@uah.es (J. Rosado-Sanz), mpilar.jarabo@uah.es (M.P. Jarabo-Amores), david.mata@uah.es (D. Mata-Moya), pedrojose.gomez@uah.es (P.J. Gómez-del-Hoyo), nerea.rey@uah.es (N. Del-Rey-Maestre).

https://doi.org/10.1016/j.ast.2020.106445

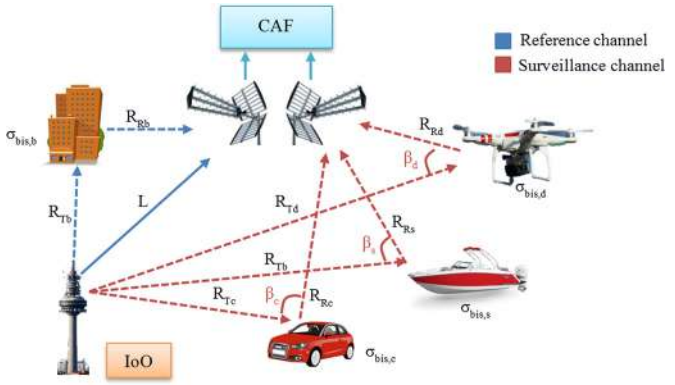

Fig. 1. Passive bistatic radar system geometry and main elements ($i \in \{b, c, d, s\}$ refers to building, car, drone and ship, respectively). (For interpretation of the colours in the figure(s), the reader is referred to the web version of this article.)

and UHF bands [5], and the UHF and the S bands [10]; arrays of discone antennas [11,13] and logarithmic periodic microstrip antennas [12,14].

The present paper focuses on the use of Digital Video Broadcasting-Terrestrial (DVB-T) transmitters as IoOs. More specifically, the surveillance antenna design problem is tackled. DVB-T signals are of great interest because of their availability, radiated powers, signal bandwidth, and waveform correlation properties [15,16,18,17]. DVB-T was allocated in the frequency band that spanned from 450 MHz to 850 MHz [19]. After the analogue switch-off, the 800 MHz band was released for LTE. In Spain, each DVB-T Mux is composed of a centred data bandwidth of 7.607157 MHz, and two adjacent guard bands to complete a 8 MHz bandwidth [19]. Main challenges to be faced in the surveillance antenna design are the following:

- The IoO signal bandwidth, B, determines PR range resolution: $\Delta Rb = c/B$, being $Rb = R_T + R_R - L$ the bistatic range, and c the speed of light.
  Multichannel DVB-T signals are used for increasing range resolution, but associated requirements are challenging due to the high relative bandwidths.
- DVB-T transmitted powers fulfil defined broadcasting service quality requirements, and give rise to weak target PR echoes that impose the use of high gain surveillance antennas to fulfil radar detection requirements.
- The Direct Path Interference (DPI), which is the direct IoO signal received by the surveillance antenna, is a critical interference source, because its level can be $80 - 100$ dB higher than the radar echoes generated by the targets to be sought. Usually, PR geometry is selected to keep the IoO at the back side of the PR surveillance antenna, which is designed to have a high Front-to-Back ratio (FB).
- To guarantee coverage sectors of interest in surveillance applications, enough angular resolution for target localization, and capability of Detection of Arrival (DoA) estimation, array processing techniques are used, which can also be designed for interference spatial filtering [20][21].

In this paper, the design and validation of a new single radiating element and a linear array for DVB-T PRs is presented. Ground targets detection is the validation problem, because car's low Doppler shifts increase the impact of DPI and clutter returns, complicating the design of radar detectors [22]. Other challenging targets are Unmanned Aerial Vehicles (UAVs) [23]. Their use in civilian applications is increasing, and opening a new problem related to the identification of collaborative and non-collaborative (friend or foe), for which detection is a critical previous stage [24].

Table 1
3D IDEPAR design parameters.

	5 elements NULA	New 7 elements array
Signal Bandwidth (MHz)	25	100
Antennas Bandwidth (MHz)	712 – 787 (10%)	690-790 (13.5%)
Gain (dBi)	6.9	> 7
Polarization	Horizontal	
Array Gain (dBi)	13.89	> 14
SLL (dB) [27]	11.6	14
Azimuth/elevation Coverage (°)	60/ – –	80/60
Angular Resolution (°)	19	< 19
Bistatic Range Resolution (m)	12	3

IDEPAR is a PR demonstrator developed in the University of Alcalá, that can employ DVB-T transmitters as IoOs [17,12]. An updated version includes eight independent acquisition chains with a maximum instantaneous bandwidth of 100 MHz, that allow the design of a seven element surveillance array (keeping the eighth acquisition chain for the reference signal). The proposed single radiating element achieves a gain higher than 7 dBi, and wide elevation and azimuth beamwidths, within a broad bandwidth of 31.8% at 700 MHz. In [25] it is shown that the element spacing affects the radiation performance of the array. The design of the Non-Uniform Linear Array (NULA) is based on a new methodology that optimize inter-element distances including coupling effects between elements with this spacing, controlling the design computational cost. The prototype was integrated in IDEPAR and validated in a real scenario in University of Alcalá external campus [12,26].

The 700 MHz DVB-T band is expected to be released for 5G, by the end of 2020. Results presented in this paper date from the beginning of 2019, when most of the signals were concentrated in the 700 MHz band, but the proposed methodologies and solutions can be applied to antenna designs at lower DVB-T frequencies, after the second frequency reallocation, and for the design of new antennas according to 5G systems requirements.

The rest of the paper is structured as follows: section 2 describes the PR demonstrator and the validation radar scenario; sections 2.1 and 2.2 define the design requirements according to PR operation; sections 3 and 4 explain the design of single radiating element and the array, including characterization in anechoic chamber and a comparative analysis of results with other works from literature; section 5 shows the integration of the designed array in IDEPAR demonstrator and the results of PR measurements in the trial scenario. Finally, the conclusions are summarized in section 6.

2. IDEPAR demonstrator and radar scenario

IDEPAR can be configured with a high gain single surveillance antenna to perform 2D detection and tracking (bistatic range, bistatic Doppler) [17,26], or with an antenna array for 3D detection and tracking (bistatic range, bistatic Doppler, azimuth) [12]. Main parameters of IDEPAR are summarized in Table 1: NULA of 5 commercial antennas [12]; updated acquisition chains and desired parameters for the new 7-elements array to be designed. The 7 elements NULA was expected to increase the Side Lobe Level (SLL), defined as the difference between the main beam level, in decibels, and the highest side lobe level, in decibels, from 11.6 dB to 14 dB, a desired feature to improve target detection and DoA accuracy.

The validation scenario is located at the rooftop of the Superior Polytechnic School of the University of Alcalá (Fig. 2) [17,26]. The IoO is Torrespaña, 28.5 km far from the PR. The ground targets to be detected are running along the Meco road, which distance with

Fig. 2. Validation scenario and desired angular coverage (blue sector).

respect to the PR varies from 300 m to 1 km, and the R2 Highway, with distances to the PR close to 2 km. Recreational drones, which, according to current regulations, can fly up to a maximum height of 120*m*, and planes that are usually observed during their landing approach to the Adolfo Suarez-Barajas airport, are also considered.

The Area of Interest (AoI) is an angular sector of at least 60° [12]. It is defined by the single radiating element azimuth beamwidth, that is increased to 80° in the new 7 elements array (Table 1). Elevation beamwidth is not critical for ground targets detection, but in the new design, a value of 60° (+30° above the array broadside) is specified for detecting drones flying at an altitude of 120 m, up to 200*m* far from the PR.

Design parameters analyzed so far are related to the required angular coverage and the available acquisition chains. In the next sub-sections, other key design parameters are studied taking into consideration array performance and range coverages.

2.1. Single radiating element physical size

The maximum size of the single radiating element along the linear array axis is defined to avoid grating lobes within the desired pointing range. Representing the Array Factor (AF) versus the distance between elements in an ULA (2), it is found that the maximum distance for the worst case (highest frequency), $N = 7$ elements and desired pointing within the angular coverage ($\theta_d = \{-40°, +40°\}$), is $d = 0.53\lambda$ (Fig. 3). As a result, the maximum size of the single radiating element measured along the direction of the linear array, is 203 mm. Despite this is an strict requirement, an smaller antenna could improve the NULA performance in terms of SLL [27].

$$|AF| = \frac{sin\left[kNd\left(cos\theta_d - cos\theta\right)/2\right]}{sin\left[kd\left(cos\theta_d - cos\theta\right)/2\right]} \tag{2}$$

2.2. Preliminary coverage studies

For the geometry defined in Fig. 1, removing the sub-index i used for identifying the different types of targets, the bistatic radar equation is expressed in (3) [2]:

$$(R_T \cdot R_R)^2 = \frac{p_{IoO} \cdot g_T \cdot g_R \cdot \lambda^2 \cdot \sigma_{bis}}{(4\pi)^3 \cdot p_R \cdot l_T \cdot l_R} \tag{3}$$

p_{IoO} is the transmitted power by the IoO, g_T and g_R are the gains of the transmitting and receiving antennas towards the target, respectively, and λ is the signal wavelength. p_R is the received power. The excess propagation losses associated to both paths are l_T and l_R. σ_{bis} was simulated employing Ansys HFSS, at DVB-T frequencies, for the most probable bistatic angle in the radar scenario: $\phi_{bis} = 50°$.

The sensitivity of the PR system, minimum received power level at the PR surveillance antenna to fulfil detection requirements, can be expressed as a function of the Signal-to-Noise-Ratio, $(S/N)_{IN}$, and the equivalent noise temperature, T_{IN}, at the surveillance antenna terminals (4) [17].

$$S_{min} = \left(\frac{S}{N}\right)_{IN} (k \cdot T_{IN} \cdot B) \tag{4}$$

where k is the Boltzmann constant, B the acquisition bandwidth, and $T_{IN} = T_a + T_{ant-con}$ is the equivalent noise temperature at the antenna terminals, with T_a and $T_{ant-con}$ the antenna and interconnection elements equivalent temperatures.

For $T_{int} = 250$ ms, the integration gain provided by the CAF, $G_{int} = 10 \cdot log_{10}(B_{signal} \cdot T_{int})$, varies from 62.8 dB for a single DVB-T Mux ($B_{signal} = 7.6$ MHz) to 73.6 dB for a set of 12 consecutive DVB-T Mux ($B_{signal} = 91.2$ MHz), being B_{signal} the signal information bandwidth. Because of that, the sensitivity will remain constant against changes in acquisition bandwidth, B, if there are a set of consecutive DVB-T channels that covers the complete acquisition bandwidth, $B_{signal} = B$. Unfortunately, this is not the case in practical situations.

The required sensitivity was calculated through system noise analysis [17], assuming a noise dominated environment and a Swerling I target model, for a minimum Probability of Detection (P_d) of 80%, and a maximum Probability of False Alarm (P_{fa}) of 10^{-6}. In Fig. 4, results are represented for $B = 100$ MHz and two B_{signal} values: $B_{signal} = 7.6$ MHz (1 DVB-T channel), and $B_{signal} = 91.2$ MHz (12 DVB-T channels).

The single radiating element and the 7-element ULA gains were assumed to be equal to 6 and 14.5 dBi, respectively. In Fig. 4, p_R is represented as a function of R_R, for cars ($\sigma_{bis,car} = 9.9$ dBsm) and drones ($\sigma_{bis,drone} = -12.4$ dBsm) for a Equivalent Radiated Power equal to 20 kW.

In the worst case, a single radiating element and 1 DVB-T Mux, cars and the considered drones can be detected up to 6 km and 1 km far from the PR, fulfilling the specified P_d and P_{fa} requirements. The better gain of the 7 element ULA increases the coverage up to 10 km for cars and more than 2 km for the drone, maintaining the integration gain of a 1 DVB-T Mux. As a result, the minimum single radiating element gain is fixed to 6 dBi.

3. Single radiating element design

A patch antenna, also called MicroStrip Antenna (MSA), is a radiating element built in a high conductivity metal over a substrate [28]. It's very attractive for modern applications because of their quasi-planar structure, light weight, compact size, easy fabrication and low cost, though they also have some important drawbacks: narrow bandwidth, low gain, poor efficiency [29][30]. Bandwidth can be enhanced employing proximity or aperture coupling techniques, instead of coaxial or microstrip lines [28], and a thick substrate with low dielectric constant ε_r [31]. Other bandwidth or gain enhancement approaches are based on modifications of the fundamental patch shape: C-patch antennas with a 3% fractional bandwidth at 2 GHz [32]; E-shaped antennas with 12% fractional bandwidth at 5 GHz [33] and 30% at 2 GHz [34]; combination of 4 notched circular patches with 3.3% fractional bandwidth at 2.4 GHz, and a peak gain of 13 dBi [35].

The following methodology is proposed for the single radiating element design: (1) selection of the patch geometry and feeding method; (2) study and application of different bandwidth enhancement techniques; (3) radiation pattern improvement through reflectors; (4) final optimization and requirements assessment.

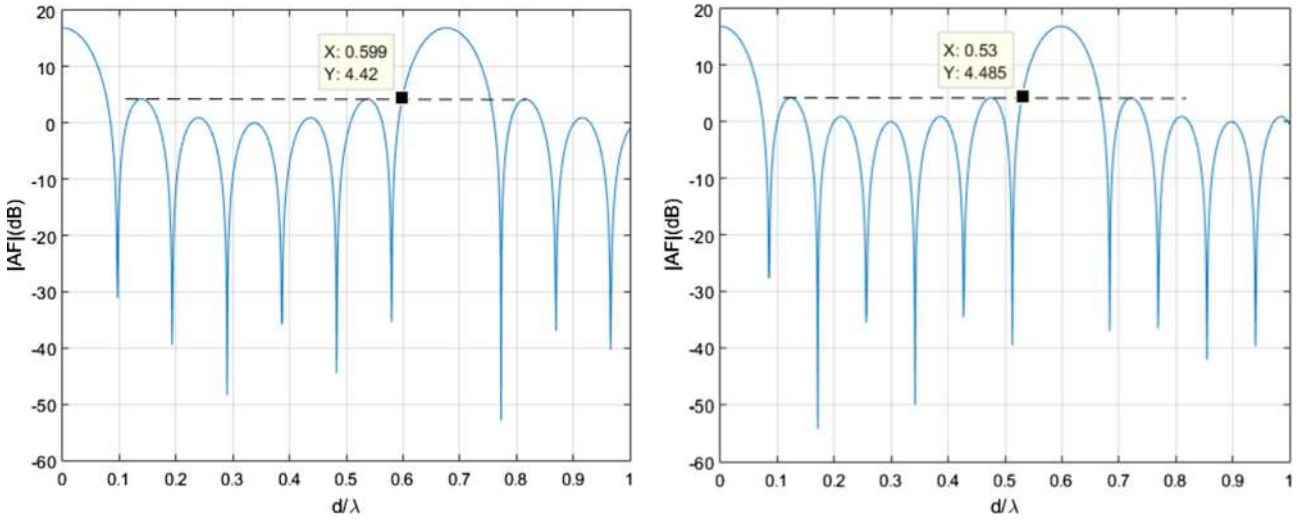

(a) 690 MHz, 1^{st} grating lobe at $d = 0.599\lambda$ (b) 780 MHz, 1^{st} grating lobe at $d = 0.53\lambda$

Fig. 3. AF for $N = 7$ and pointing direction $\theta_d = 40°$.

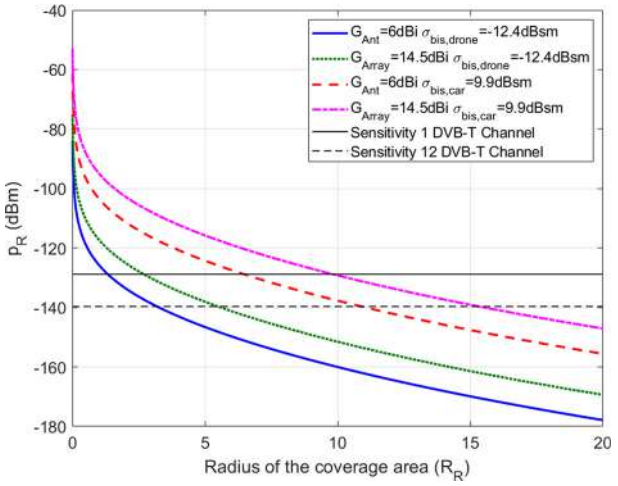

Fig. 4. Estimated coverage curves in the radar scenario for cars and drones, at 770 MHz for $P_d = 80\%$ and $P_{fa} = 10^{-6}$: single antenna ($G = 6$) dBi, and 7 elements ULA ($G = 14.5$ dBi).

A circular patch of radius $r = 56$ cm (5) (6) over FR4 substrate of a thickness h, with proximity coupling feeding through a microstrip line with characteristic impedance of 50Ω between both equal substrates, was the base design [28]. Simulation results showed that the antenna was matched at 740 MHz, the central frequency of the desired frequency band, but with a 2% bandwidth, far from the desired 13.5% (Table 1).

$$r = \frac{F}{\sqrt{1 + \frac{2 \cdot h}{\pi \cdot \varepsilon_r \cdot F} \cdot \left[log\left(\frac{\pi \cdot F}{2 \cdot h}\right) + 1.7726 \right]}} \tag{5}$$

$$F = \frac{8.791 \times 10^9}{f_0 \cdot \sqrt{\varepsilon_r}} \tag{6}$$

3.1. Bandwidth enhancement techniques

Taking into consideration that antenna bandwidth is inversely proportional to ε_r, and directly proportional to its thickness [31], a substract-less antenna was selected. The FR4 was replaced by a thick air substrate providing a bandwidth increase up to 5.4% (Fig. 5(a) blue trace).

Feeding was changed to aperture coupling. The ground plane was placed between the feed line and the substrate below the patch, with a slot which dimensions and position were calculated through optimization techniques. The resulting relative bandwidth was significantly better: 11.5% (Fig. 5(a) red trace). Fig. 5(b) shows the gain patterns: $G = 8$ dBi and elevation beamwidth of 68°, fulfilling the defined requirements (> 7 dBi and $> 60°$, respectively); azimuth beamwidth lower than the required 80°, and a low $FB \simeq 7$ dB (Table 1).

3.2. Study of reflectors for FB ratio improvements

To achieve an azimuth beamwidth greater than the elevation one, the reflector dimension along the elevation plane must be higher than along the azimuth one. Considering the maximum dimension of the single radiating element along azimuth of 203 mm (section 2.1), the maximum reflector dimensions are defined as 20 cm (azimuth) × 40 cm (elevation). Three different types were studied: plane, pyramidal and boxed (Fig. 6).

Boxed shape reflector is a novel technique proposed in [36] with interesting results. In order not to obstruct the connector, the feeding line was blended in L-shape (Fig. 6), which allowed to reduce the width of the feeding line to $w_{feed} = 5$ mm. Each reflector type improved different parameters (Fig. 7): the plane and the pyramidal reflectors improved the FB ratio to 30 dB and 25 dB, respectively, but the azimuth beamwidths were lower than 80°. The boxed reflector reached 80° of azimuth beamwidth, lower FB ratio, and the best SLL, which is expected to benefit the array performance. The maximum gain was a bit lower, but fulfilling requirements, so this reflector was the selected for the single radiating element. An important effect of the use of reflectors is the deterioration of the reflection coefficient (Fig. 8); because of that, the feeding technique was modified.

3.3. Input impedance bandwidth

A well designed H-shape slot can increase the relative bandwidth up to 30%, extending over a frequency band of more than 200 MHz (Fig. 10). The physical parameters of the H-shape slot were selected through gradient optimization to minimize $|S_{11}|$ in the desired DVB-T frequency band (Fig. 9). The reflection coefficient is below −10 dB from 578 MHz to 802 MHz, including the desired band 690-790 MHz (Fig. 10), which gives margin for manufacturing tolerances.

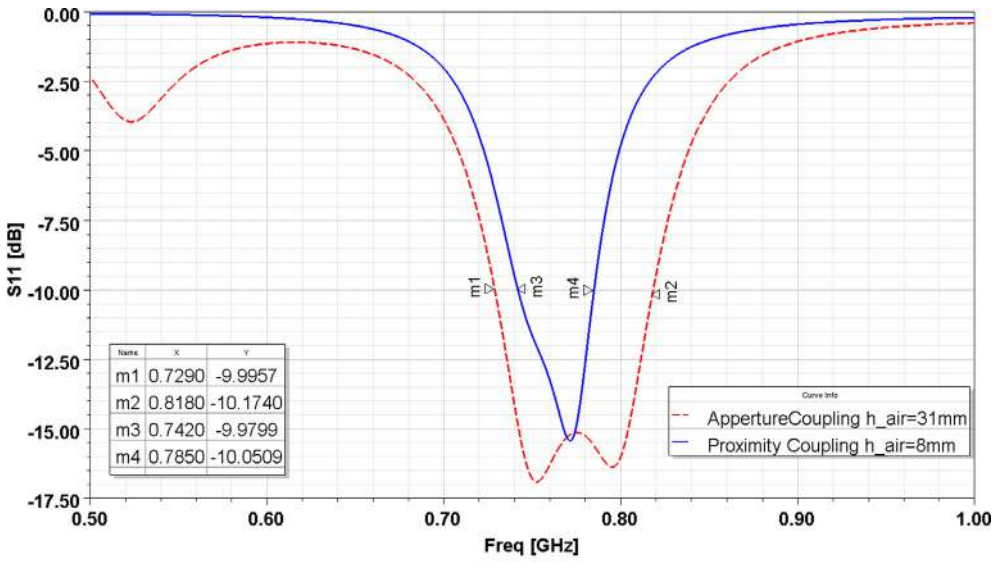

(a) $|S_{11}|$

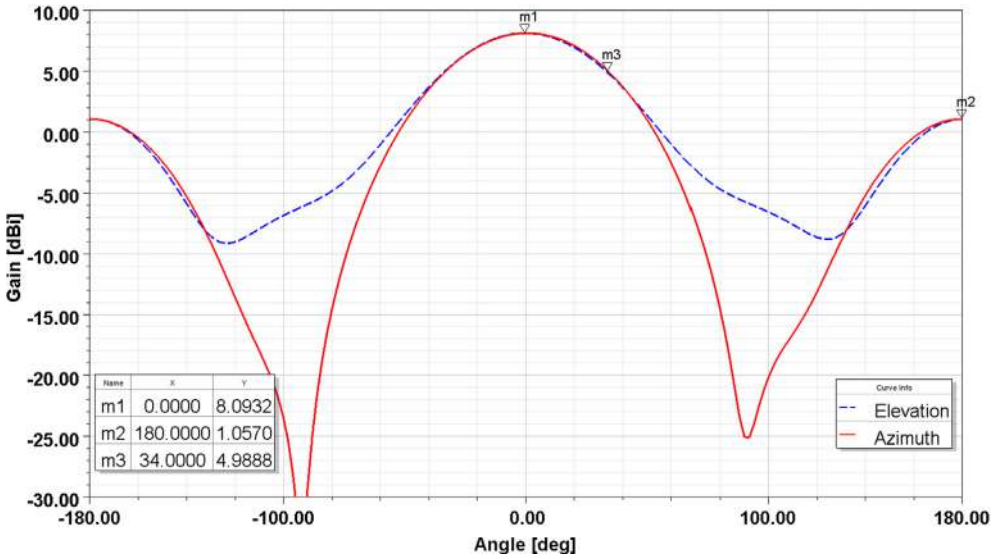

(b) Gain pattern at 760 MHz

Fig. 5. (a) $|S_{11}|$ of a circular patch antenna feed with a proximity coupling microstrip and air substrate of 8 mm (blue); basic slot aperture coupling with air substrate of 31 mm (red). (b) Elevation (blue) and azimuth (red) gain patterns for the slot aperture coupling based solution.

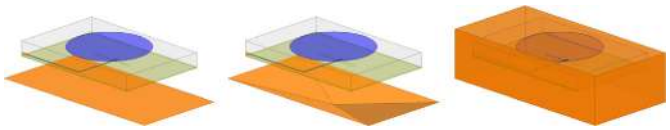

(a) Plane Reflector (b) Pyramidal Reflector (c) Boxed Reflector

Fig. 6. Reflectors studied for FB ratio and azimuth beamwidth improvement.

Adding a substrate on top of the patch provides protection against environmental elements and simplifies the manufacture of the antenna. This technique, called inverse substrate, in combination with an slot in one side of the patch, allowed to improve matching, dropping $|S_{11}|$ below -14 dB from 589 MHz to 795 MHz (29.8% of relative bandwidth, Fig. 11), leaving a 4 dB margin for manufacturing deterioration with respect to the typical -10 dB used for defining the antenna bandwidth. The substrate employed was Arlon CuClad 250GT of 0.9 mm of thickness, because it has a low dielectric constant ($\varepsilon_r = 2.5$). The dimensions of the slot were $W_{slot} = 40$ mm and $L_{slot} = 45$ mm. With these last touches the antenna fulfilled all requirements. Actually, the bandwidth was higher, spreading towards lower frequencies, where more DVB-T Muxs were expected, providing more robustness with respect to the availability of DVB-T channels. The radiation pattern shows that azimuth and elevation beamwidths fulfil the required values, with a gain and FB ratio of 7.4 dBi and 15 dB, respectively, (Fig. 12).

3.4. Final antenna design and characterization

The final prototype is presented in Fig. 13; the schematic and final dimensions in Fig. 14. During all the design process, it was verified that polarization was parallel to the feeding line coming into the patch. Because of that, the 90° rotation of the prototype guarantees the required horizontal polarization. The antenna was characterized in the anechoic chamber of the *High Technology and Homologation Centre (CATECHOM)* of the University of Alcalá (Fig. 15).

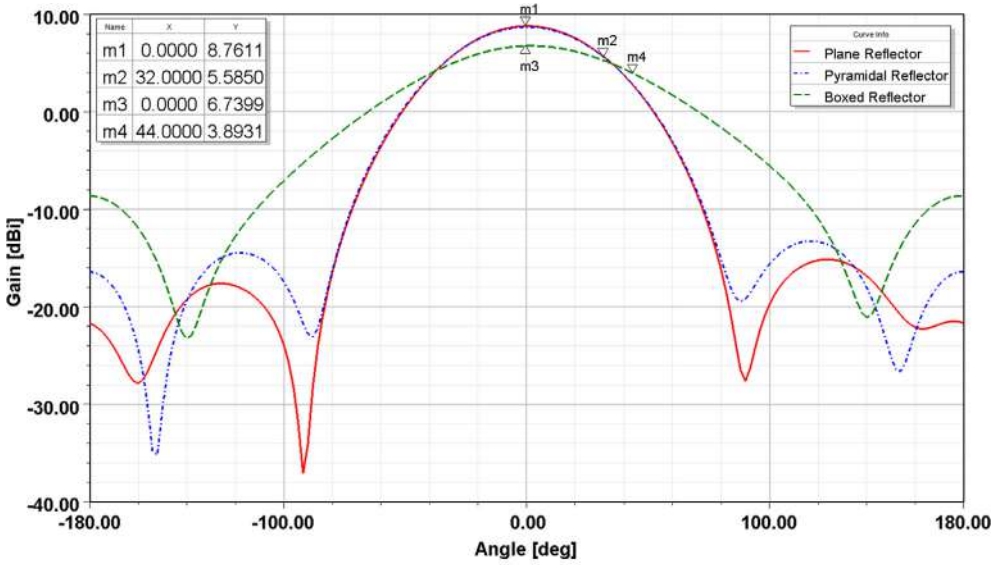

(a) Azimuth

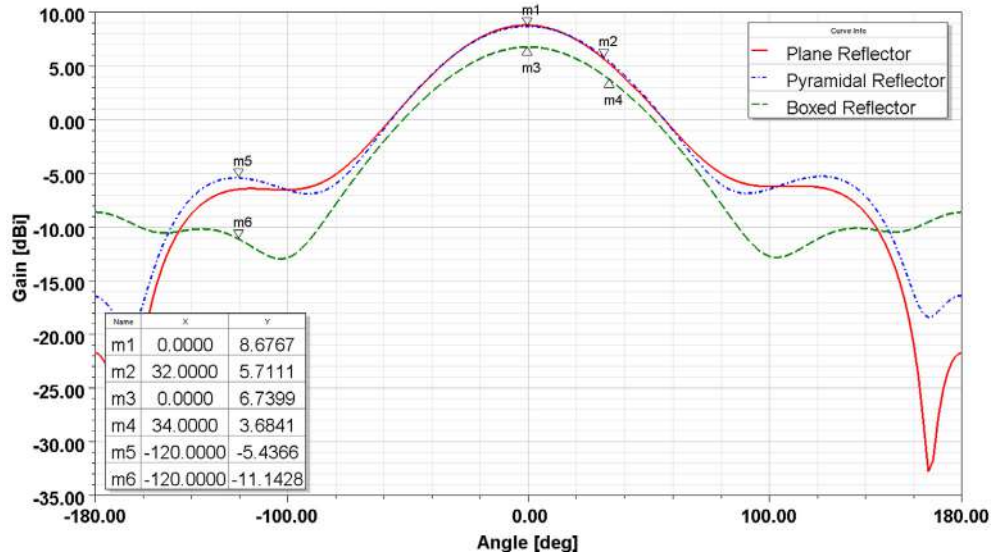

(b) Elevation

Fig. 7. Gain patterns for different shape reflectors at 760 MHz.

Measured $|S_{11}|$ is shown in Fig. 16 verifying that the relative bandwidth is 31.8%, for $|S_{11}| < -10$ dB, which surpassed the desired minimum value of 13.5% (Table 1) and provides to the PR system the possibility of selection of the frequency band that contains more DVB-T channels in each location, improving system capabilities.

The radiation pattern was measured in the front hemisphere, because of the positioner blocking effect. Azimuth and elevation beamwidths were a bit wider than simulated ones, and gain was lightly reduced to a maximum of 6.5 dBi (Fig. 17).

4. Non-uniform linear array design

The main advantage of NULA v.s. ULA, is the possibility of improving SLL [27,37]. A high SLL is important in all communications systems, and also in radar, because of its impact on target angular discrimination capability. Optimization algorithms were used to determine the inter-element spacings ($\mathbf{d} = [d_{12}, d_{23}, d_{34}, d_{45}, d_{56}, d_{67}]$) that minimized the SLL controlling the directivity (Fig. 18). d_{ij} in $\mathbf{d}$ could vary from $d_{min} = 201$ mm (defined by the physical dimension of the single radiating element along the axis of the antenna array), and $d_{max} = 0.56\lambda$, for avoiding grating lobes in an ULA at the considered central frequency (740 MHz) for a steering sector ranging from $-40°$ to $40°$: $d_{max} = 227$ mm.

The optimization algorithm described in [12] was revisited and modified to include coupling effects between elements. The proposed cost function is expressed in (7) and (8).

$$\bar{C}_{sll_{max},\mathbf{\Phi}_{AoI}}(\mathbf{d},k) = \frac{1}{N_{\mathbf{\Phi}_{AoI}}} \sum_{i=1}^{N_{\mathbf{\Phi}_{AoI}}} C_{\phi_{AoI,i}}(\mathbf{d},k,sll_{max}) \tag{7}$$

$$C_{\phi_{AoI,i}(\mathbf{d},k,sll_{max})} = \sum_{\substack{\phi \notin BW_{3\,\mathrm{dB}} \\ |\bar{\mathbf{E}}(\phi,\mathbf{d})| > sll_{max}}} \left| |\bar{\mathbf{E}}_{\phi_{AoI,i}}(\phi,\mathbf{d})| - sll_{max} \right| + k \cdot BW_{3\,\mathrm{dB}}(\mathbf{d}) \tag{8}$$

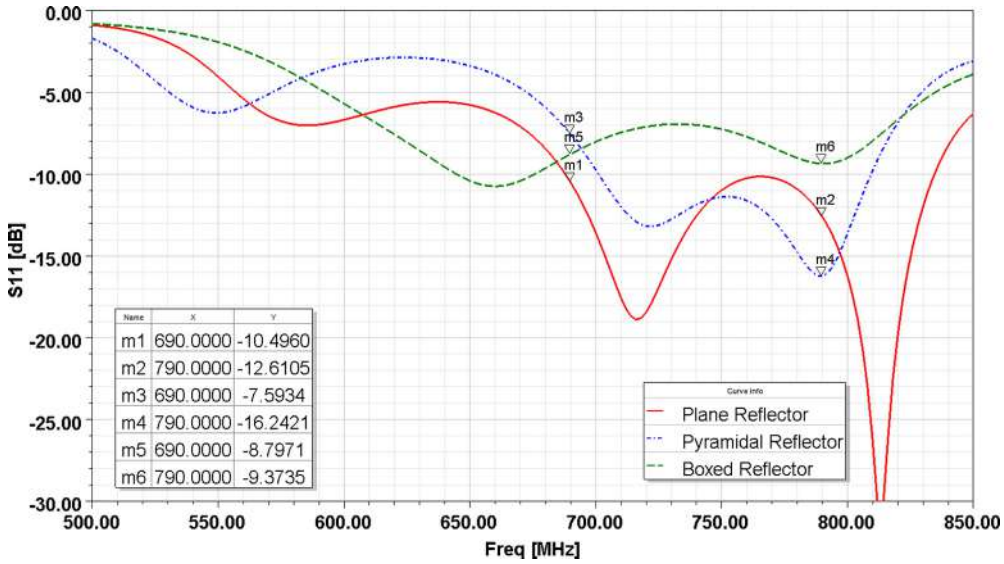

Fig. 8. Reflection coefficients of the antenna with different shape reflectors.

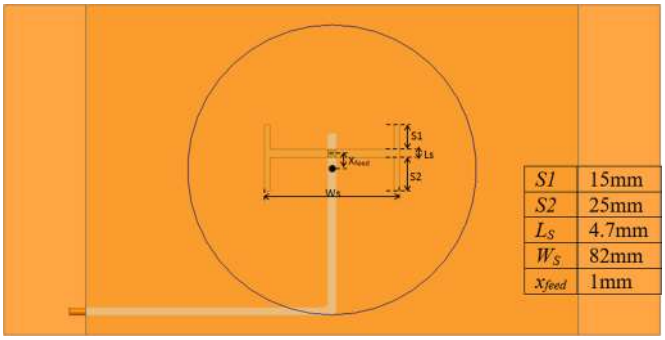

Fig. 9. H-shape aperture antenna scheme and optimized parameters.

- sll_{max} is the specified maximum side lobe level in natural units ($SLL = 10 \cdot log_{10}(sll)$) and $\mathbf{\Phi}_{AoI}$ defines the set of $N_{\mathbf{\Phi}_{AoI}}$ steering directions throughout the AoI: $\mathbf{\Phi}_{AoI} = \{\phi_{AoI,1} ... \phi_{AoI,N_{\mathbf{\Phi}_{AoI}}}\}$.
- $\mathbf{d}$ is the inter-element distances vector (Fig. 18); k controls the main beam width, $BW_{3\,\mathrm{dB}}(\mathbf{d})$, which depends on the current $\mathbf{d}$. k was a design factor in [12], determined experimentally. In this work, it is a new optimization variable.
- $|\bar{\mathbf{E}}_{\phi_{AoI,i}}(\phi, \mathbf{d})| = \frac{|\mathbf{E}_{\phi_{AoI,i}}(\phi,\mathbf{d})|}{|\mathbf{E}_{\phi_{AoI,i}}(\phi,\mathbf{d})|_{max}}$ is the magnitude of the normalized azimuth plane radiation pattern of the array pointing towards $\phi_{AoI,i}$ [38], for the current $\mathbf{d}$. The real radiation patterns of the elements integrated in the NULA are employed for calculating $\mathbf{E}_{\phi_{AoI,i}}(\phi, \mathbf{d})$, with the objective of including electromagnetic coupling effects during the optimization process.

4.1. Coupling effects modelling and optimization process

Due to the wide variety of possible architectures, real radiation patterns of the elements in the array were approximated through simulations using ANSYS HFSS. Two ULAs were generated with inter-element distances $d_{ULA_1} = 201$ mm ($\sim 0.5\lambda$ @740 MHz) and $d_{ULA_2} = 230$ mm ($\sim 0.56\lambda$ @740 MHz), respectively. In both cases, non-ending elements had very similar radiation patterns, but different from the ending ones (Fig. 19). These results were used for reducing computation complexity in the optimization of inter-element distances. The simulated central element radiation pattern was used for the rest of non-ending elements, considering the distances to their neighbours; simulated radiation patterns of the ending elements were preserved, taking into consideration the different distances to their neighbours.

Table 2
Number of simulations needed as a function of the number of possible distances between elements (N_d) for complete and simplified methods.

Method	$N_d = 3$ $\Delta d \approx 0.08\lambda$	$N_d = 5$ $\Delta d \approx 0.04\lambda$	$N_d = 7$ $\Delta d \approx 0.025\lambda$
Complete	$3^6 = 729$	$5^6 = 15625$	$7^6 = 117649$
Simplified	$3^2 + 2 \cdot 3 = 15$	$5^2 + 2 \cdot 5 = 35$	$7^2 + 2 \cdot 7 = 63$

A direct search method called *General Pattern Search* was employed. A set of $N_d = 7$ distances in the interval $[d_{min}, d_{max}]$ was used to define the search grid, $\mathbf{d}_{search}$, with an uniform separation of Δ_d (9).

$$\min_{\mathbf{d},k} \bar{C}_{sll_{max},\mathbf{\Phi}_{AoI}}(\mathbf{d}, k) \qquad \mathbf{d} \in \mathbf{d}_{search} \tag{9}$$

For a NULA design the maximum distance between elements could be greater than the one studied for an ULA in order to avoid grating lobes, because the design optimization process will allow to avoid them. The optimization algorithm sets off from an initial point (initial solution), takes different points surrounding the actual one, and evaluates the associated cost function values. The point with the lowest associated cost is selected as the starting one for the next iteration. The algorithm will stop when no cost reduction is achieved [39].

Table 2 summarizes the number of simulations required for generating the single elements' radiation patterns to be used by the direct search method. Results reveal a significant reduction in computational burden associated to the simplified approach based on the use of the central element radiation pattern for the rest of non-ending elements of the array, and preserving the simulated radiation fields generated for the edge elements.

4.2. Results

The methodology and results presented in [12] are considered as reference. Four different designs were performed to analyse the improvements associated to the proposed single radiating element (section 3) and the modification of the NULA design including coupling effects controlling the associated computational cost (section 4.1):

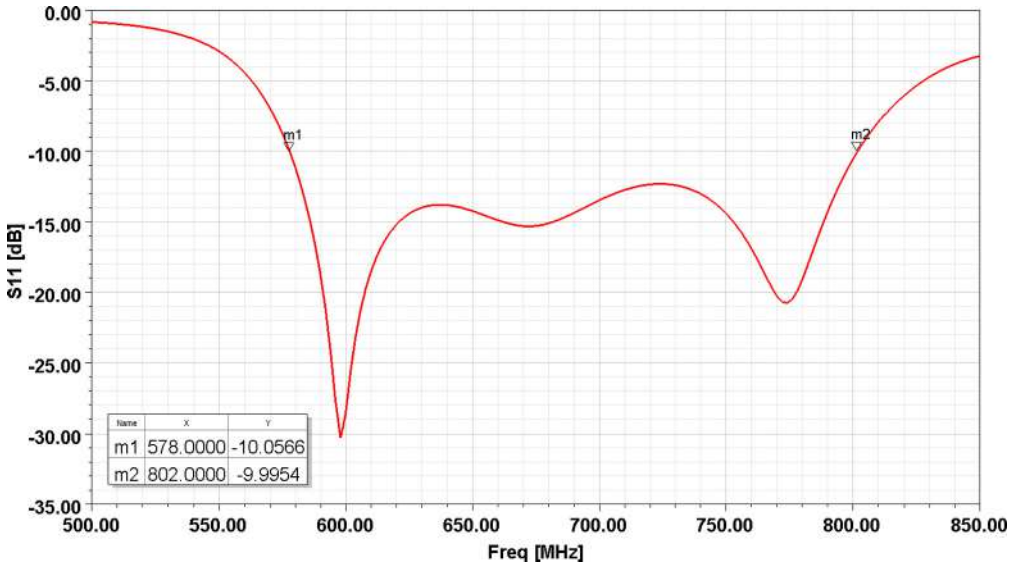

Fig. 10. $|S_{11}|$ of circular patch antenna with thick air substrate, H-shape aperture coupling feeding and boxed reflector.

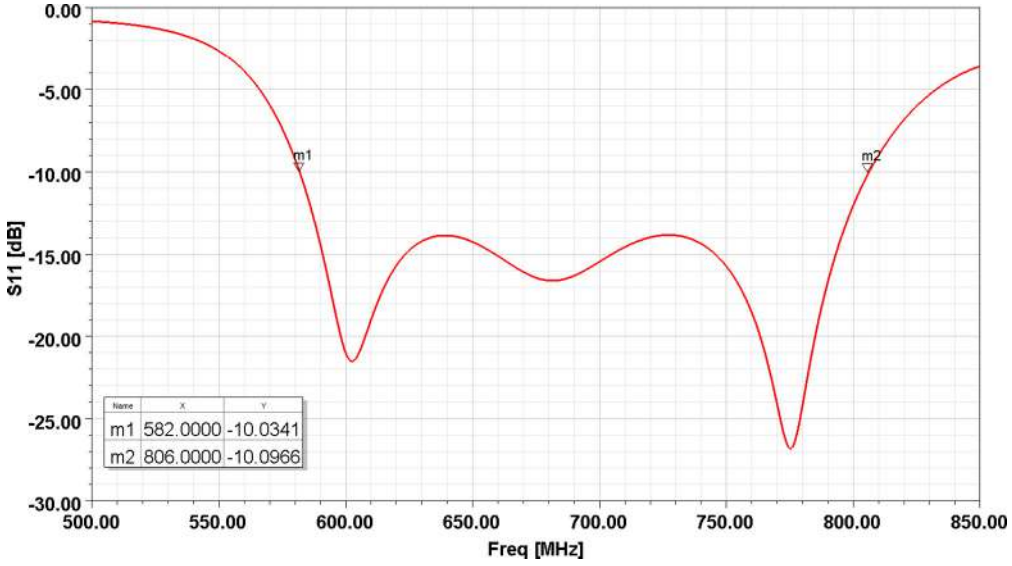

Fig. 11. $|S_{11}|$ of the circular inverted patch antenna with slot, thick air substrate, H-shape aperture coupling feeding and boxed reflector.

Table 3
Main parameters of the different arrays at $f = 740$ MHz.

Parameter	$NULA_{DA}$ [12]	$NULA_{4G}$ [12]	$NULA_{DA}$	ULA_{DA}
$G_{\phi_{Aoi}=0°}$	15.1 dBi	13.8 dBi	15.2 dBi	15.3 dBi
$BW_{3\,dB\_\phi_{Aoi}=0°}$	14°	12°	14°	14°
$SLL_{\phi_{Aoi}=0°}$	14.1 dB	14 dB	14.8 dB	12.9 dB
$G_{\phi_{Aoi}=\pm30°}$	14.5 dBi	12.8 dBi	14.5 dBi	14.6 dBi
$BW_{3\,dB\_\phi_{Aoi}=\pm30°}$	15°	15°	15°	15°
$SLL_{\phi_{Aoi}=\pm30°}$	12.9 dB	11.8 dB	13.4 dB	11.3 dB

- $NULA_{DA}$ [12]: the prototype antenna proposed in section 3 was used to design a NULA according to the method proposed in [12]. To model the radiation pattern of each single radiating element in the NULA, an ULA with inter-element distance equal to $d_{min} = 201$ mm was simulated, and the pattern of the central element was used for all the elements in the NULA. After the optimization process $\mathbf{d} = [254.8, 206.2, 201, 201, 233, 201]$ mm (Fig. 20, Table 3). In the worst case (first column of Table 3), SLL = 12.9 dB was achieved, for beams pointing to $\pm30°$ with respect to the array broadside in the azimuth plane.
- $NULA_{4G}$ [12]: In this design, the same methodology as that explained for the $NULA_{DA}$ [12] was applied, but the prototype antenna was substituted by a commercial one (Televes 4GNOVA). The associated gain and SLL were worse than those obtained with the proposed single radiating elements (SLL = 11.8 dB; Gain = 12.8 dBi) and the total aperture length increased (second column of Table 3).
- $NULA_{DA}$: A third NULA was designed using the method and the single radiating element proposed in this paper. Inter-element distances were $\mathbf{d} = [229.4, 219.6, 201, 201, 201, 255]$ mm. Results are shown in and Fig. 21 and in the third column of Table 3. It is proved that the inclusion of coupled patterns improves the SLL at least 0.5 dB.
- ULA_{DA}: An ULA of the same aperture length than $NULA_{DA}$, i.e. inter-element distance equal to the mean of distances of $NULA_{DA}$, was analyzed for comparison purposes. Results showed that the SLL decreased to 11.3 dB in the worst case, maintaining the directivity (Fig. 22, and second column of Table 3).

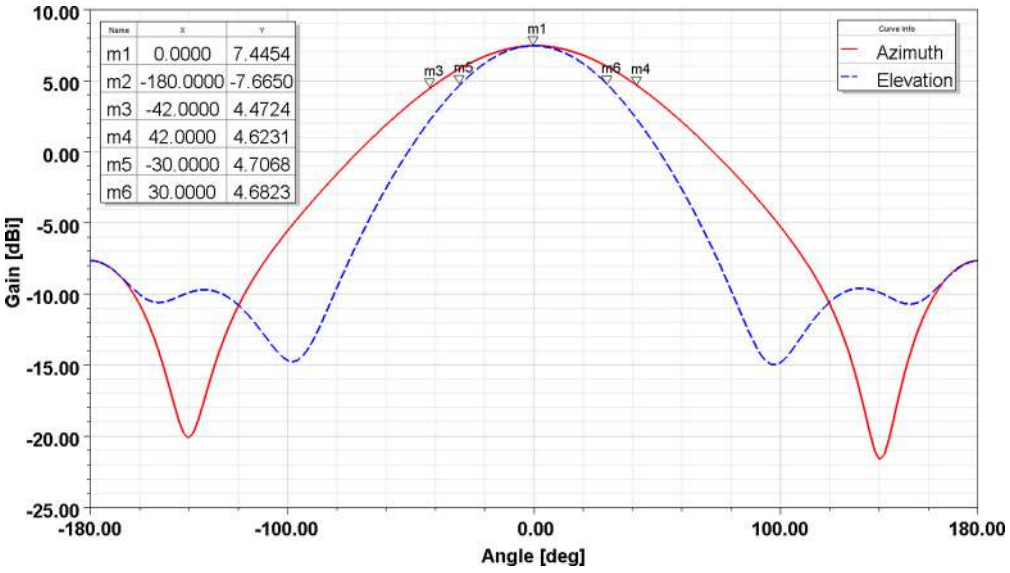

Fig. 12. Radiation pattern at 760 MHz of the circular inverted patch antenna with slot, thick air substrate, H-shape aperture coupling feeding and boxed reflector.

Table 4
Results from the comparative analysis with other methods in literature. For the proposed $NULA_{DA}$, parameters for $\phi_{AoI} = 0°$ are included to perform the comparison in similar conditions. *ND* means *Not Defined* in the related reference.

Array antenna	$NULA_{DA}$	[9]	[11]	[13]	[14]	[35]
Array type	Linear	Circular	Linear	Circular	Linear	Planar
Single element (SE)	proposed MSA	Biquad	Discone	Discone	Log Periodic	MSA
SE Dimensions	200 mm × 400 mm	500 mm × 500 mm	$\oslash = 200$ mm	$\oslash = 200$ mm	340 mm × 600 mm	$\oslash = 46.75$ mm
Number of elements	7	8	11 (13)	11	8	4
SE Gain	6.5 dBi	10 dBi	2.96 dBi	2.96 dBi	7.5 dBi	ND
Central frequency	691 MHz	650 MHz	675 MHz	675 MHz	630 MHz	2.45 GHz
Relative bandwidth	31.8%	30.7%	67%	67%	50%	3.3%
Beamforming type	Conventional	Conventional	Conventional	LMS Bucci	Conventional	Conventional
Gain	15.2 dBi	ND	17.5 dBi	ND	15 dBi	13 dBi
SLL	14.8 dB	7 dB ($\overline{SLI} = 0.8$)	13 dB	16 dB	$10 - 15$ dB	25 dB
$BW_{3\ dB}$	14°	ND	8°	30°	10°	40°

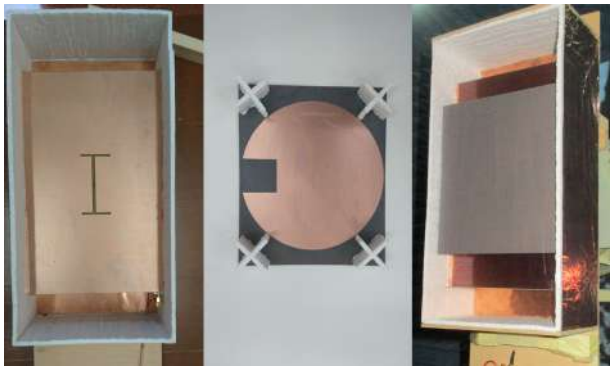

Fig. 13. Final antenna prototype showing the assembly of: the reflectors, ground and feeding layers (left), the patch with inverse substrate technique (centre) and final assembled prototype (right).

4.3. Comparative analysis with other methods in literature

In Table 4 main figures of antenna array solutions proposed in literature are summarized. UHF PR designs, and solutions for other frequency bands are included. The number and type of single radiating elements, the array architecture and the beamforming techniques for array pattern formation are also relevant factors included in the comparative analysis.

In [9] a circular array of 8 high gain biquad antennas is presented. The array includes a cylindrical reflector to improve radiation properties, and operates in UHF band with a 30% relative bandwidth.

LORA 11 is an array of discone antennas for a DVB-T passive Radar [11]. The relevance of the FB ratio in the considered application is brought to light through the use of a block of absorbent material to prevent the back radiation, probably to mitigate the effect of the DPI. It is composed of 13 antennas, but only the 11 central ones are used. This could be motivated for the different radiation properties of the ending elements in the linear array. In the present work, all available single radiating elements are used, thanks to the inclusion of the radiation pattern of each element, in presence of the rest of elements of the array, in the optimization process (section 4.1). The same single radiating element is employed to generate a circular array, CORA 11, improving SLL, but widening the array beamwidth [13].

SMARP system is a DVB-T passive radar that employs a linear array of 8 log-periodic dipole antennas [14]. Provided antenna radiation parameters fulfil the defined requirements. The inter-element spacing of 300 mm is lower than the horizontal dimension of the antenna for horizontal polarization. Coupling effects could be of relevance. At the central frequency, this distance is higher than $\lambda/2$, and the electrical inter-element distance increases with frequency, which could limit the array steering margin.

The MSA planar array proposed in [25] operates between 2.41 and 2.49 GHz, a frequency band comprising frequencies higher than those considered so far. The estimated relative bandwidth is 3.3%, and the rotation of each single circular element provides high SLL reduction.

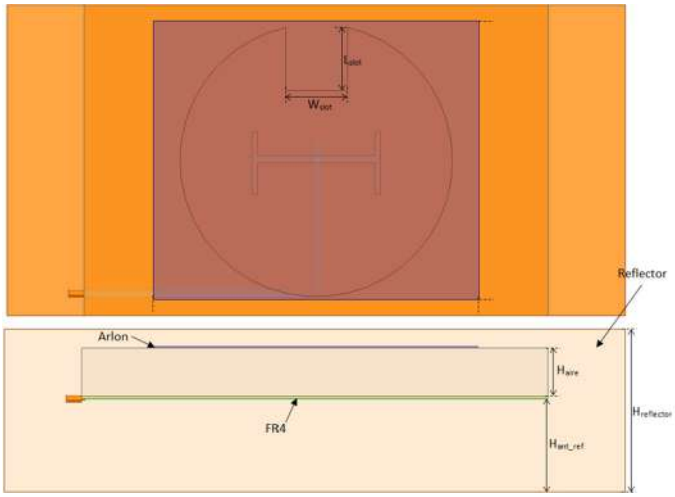

Arlon	180mm x210mm x0.9mm
FR4	200mm x300m x1.6mm
Reflector	200mm x400mm x104.9mm
Radius	88mm
Lslot	45mm
xfeed	1mm
S1	15mm
S2	25mm
Ls	4.7mm
Ws	82mm
W_{slot}	40mm

Fig. 14. Final antenna design.

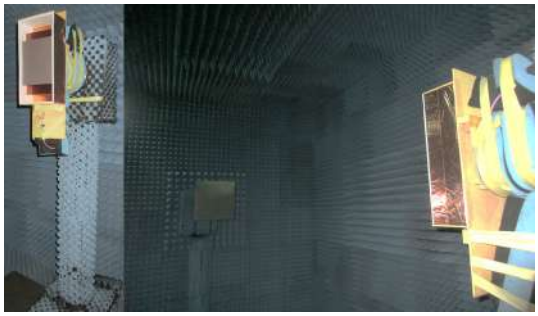

Fig. 15. Prototype antenna characterization in anechoic chamber.

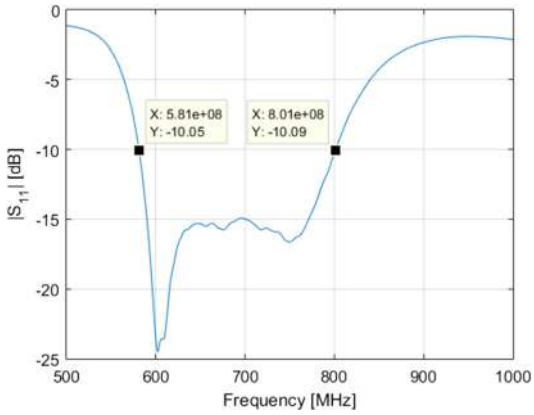

Fig. 16. Measured $|S_{11}|$.

This comparative study allows to conclude about the interest in the design of array antennas in UHF, and the relevance of the defined design requirements, that justify the presented research work. Further design efforts are expected to be encouraged by the new requirements defined by 5G communication services that will operate in the 800 MHz band.

5. Validation in IDEPAR measuring campaigns

The designed array was manufactured and integrated in the IDEPAR demonstrator (Fig. 23). Measurement campaigns were carried out in the radar scenario described in section 2.

The processing chain described in [12] was used, with an ECA filter to mitigate the effect of DPI [40]. Main parameters are summarized in Table 5. Data acquisitions of $T_{acq} = 20$ s were processed

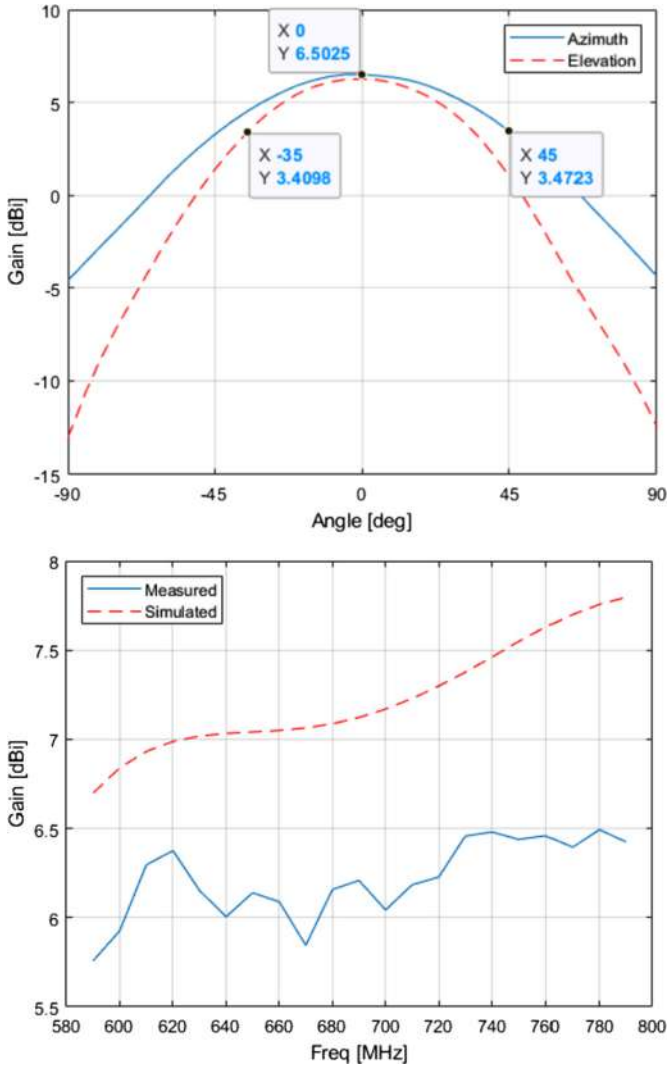

Fig. 17. Antenna measurements: cuts at 760 MHz (top); maximum gain (bottom).

in consecutive CPIs of $T_{int} = 250$ ms (bistatic Doppler resolution of 4 Hz). The acquisition bandwidth of 25 MHz gave rise to a bistatic range resolution of 12 m. The azimuth radiation pattern and covered area for the surveillance beam pointing to $\phi_{AoI} = -16.5°$ are shown in Fig. 24.

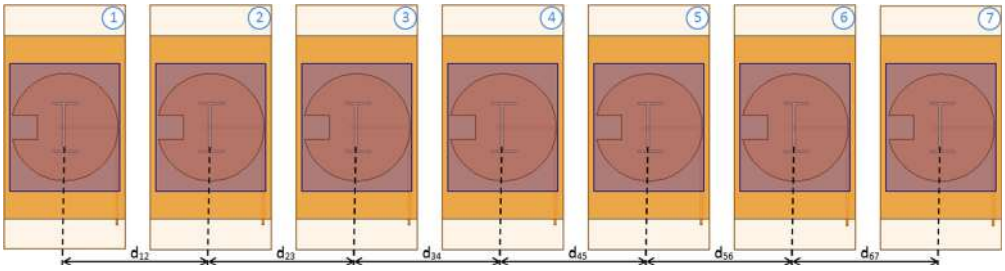

Fig. 18. 7 elements NULA with inter-element spacing $\mathbf{d} = \{d_{12}, d_{23}, d_{34}, d_{45}, d_{56}, d_{67}\}$.

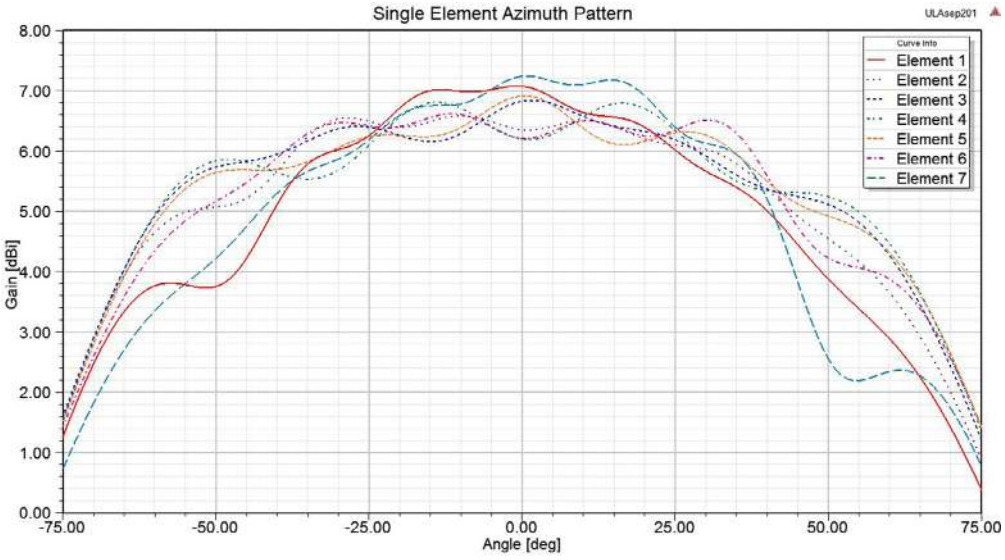

(a) ULA d = 201 mm

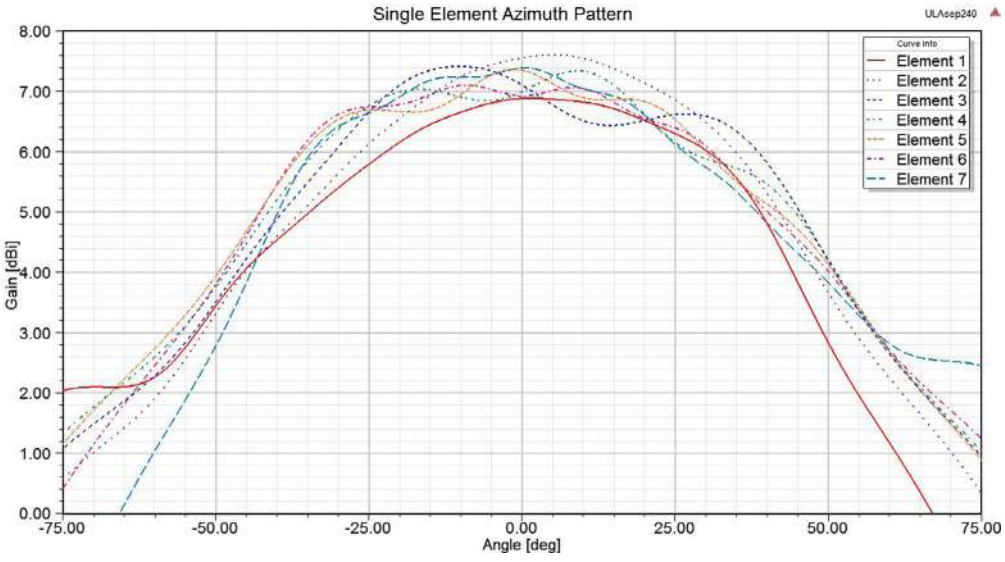

(b) ULA d = 230 mm

Fig. 19. Comparison of single elements' azimuth patterns for an ULA, including electromagnetic coupling effects.

In Fig. 25 the maxima of CAF intensity through all the acquisition time, calculated at bistatic range-Doppler cell level, are shown for the beam pointing towards $\phi_{AoI} = -16.5°$. Fig. 26 depicts the superposition of the 80 CFAR detection matrices generated throughout all the acquisition time. The CA-CFAR estimated the detection threshold using a 3D reference window (range, Doppler and azimuth) [12]. Ground targets were detected in Meco road and R2 highway; an aerial target was detected at further distances in landing approach. The targets were controlled by visual inspection, because in these roads there is not heavy traffic.

The Signal-to-Interference Ratio (SIR) before the detector was estimated for targets in different scenario areas: a car in Meco Road presented a mean SIR of 23.7 dB, a car in R2 a SIR of 22.31 dB, and the plane had a SIR of 20.81 dB. Taking into consideration that a SIR = 17.8 dB is required for fulfilling the specified detection performance requirements, $P_d = 80\%$ and $P_{fa} = 10^{-6}$, assuming a

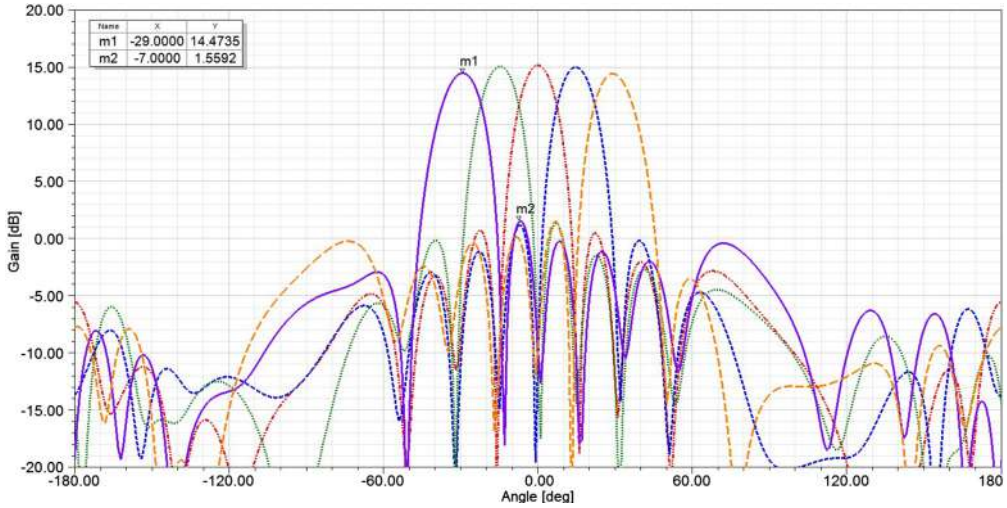

Fig. 20. $NULA_{DA}$ [12] design: $\mathbf{\Phi}_{AoI} = \{-30°, -15°, 0°, 15°, 30°\}$, f = 740 MHz.

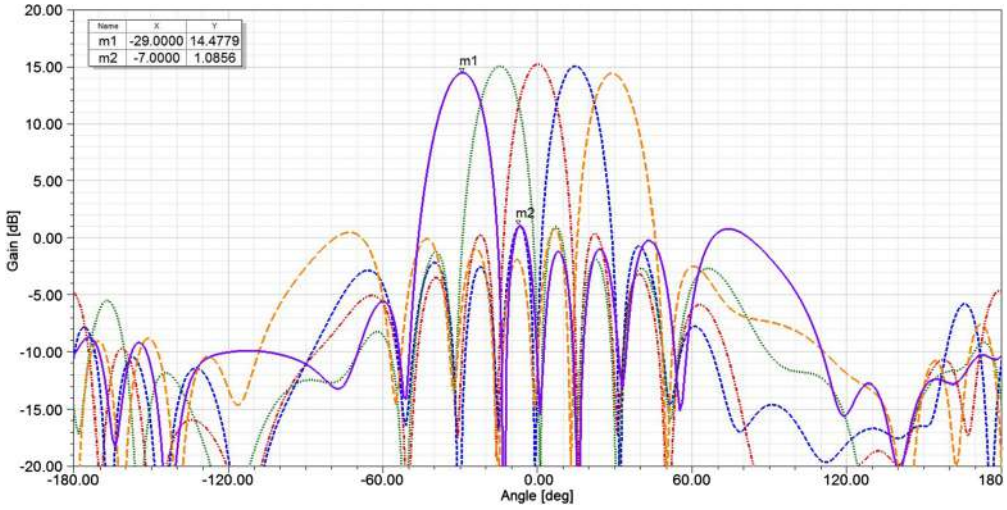

Fig. 21. Azimuth radiation pattern of $NULA_{4G}$ [12]: $\mathbf{\Phi}_{AoI} = \{-30°, -15°, 0°, 15°, 30°\}$ and $f = 740$ MHz.

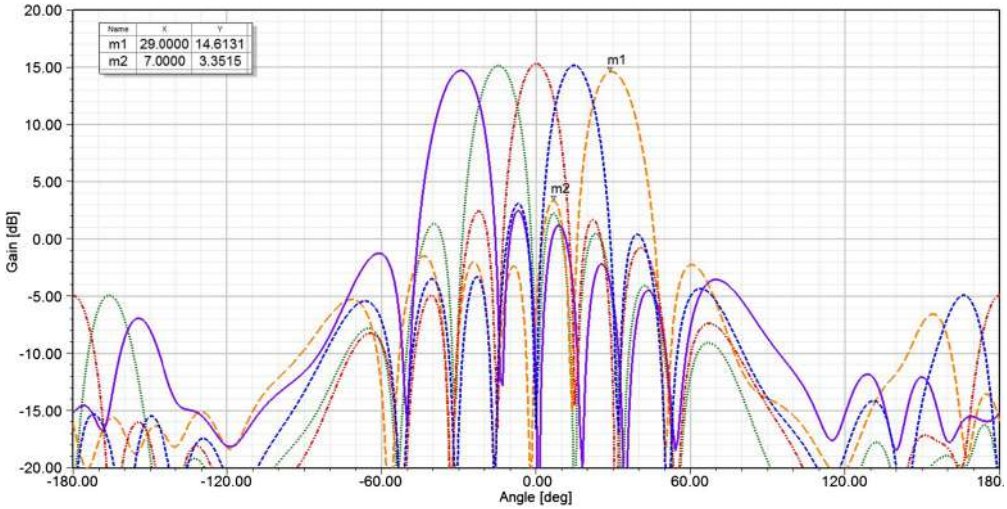

Fig. 22. Azimuth radiation pattern of ULA of same aperture length than the second NULA for $\mathbf{\Phi}_{AoI} = \{-30°, -15°, 0°, 15°, 30°\}$ at $f = 740$ MHz.

Fig. 23. Designed array integrated in IDEPAR demonstrator in the radar scenario.

Table 5
Acquisition and processing parameters of radar measurement.

Central Frequency	698 MHz
Bandwidth	25 MHz
T_{acq}	20 s
T_{int}	250 ms
Range Resolution	12 m
Doppler Resolution	4 Hz

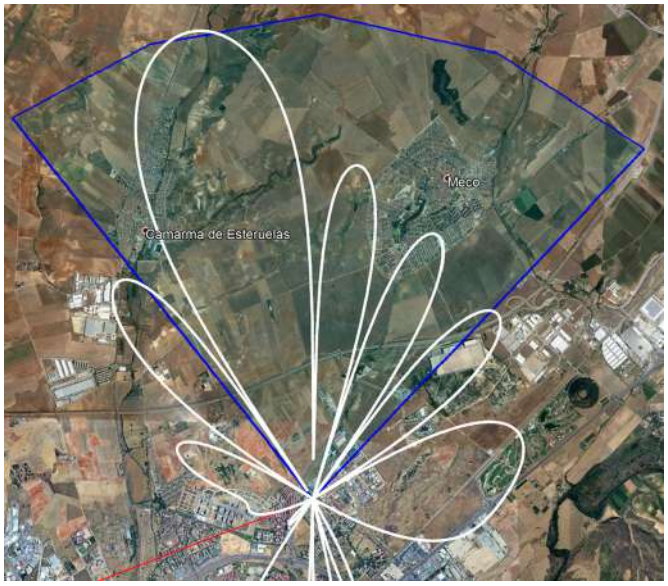

Fig. 24. Azimuth radiation pattern and covered area for $\phi_{AoI} = -16.5°$.

noise dominated environment and a Swerling I target model [17], further targets of similar characteristics could be detected.

After applying DoA techniques to the detected tracks, targets trajectories can be projected on a map [12]. Results are shown in Fig. 27, where the tracks corresponding to ground targets follow the two main roads. The furthest detected targets are the plane, which is at almost 6 kms from the PR, and a car along R2 at 2 km from PR ($R2$ *track*1). According to coverage studies presented in section 2.2, a car could be detected at a maximum distance of 12 km from PR, employing the same 3 DVB-T channels.

6. Conclusions

A broadband microstrip antenna was designed for being used as single radiating element of the surveillance channel antenna array of a passive radar system exploiting DVB-T as IoO (UHF band). An-

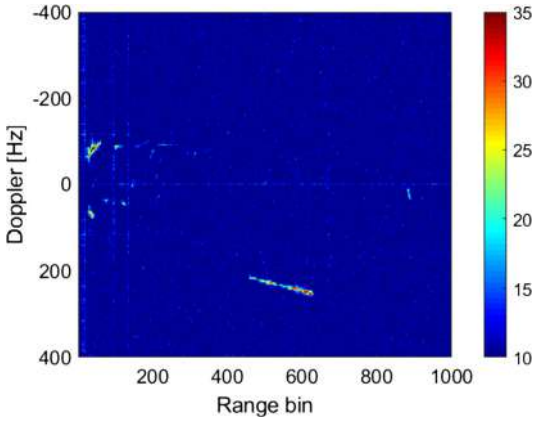

Fig. 25. CAF intensity maxima throughout all the acquisition time at bistatic range-Doppler cell level. Surveillance beam pointing towards $\phi_{AoI} = -16.5°$.

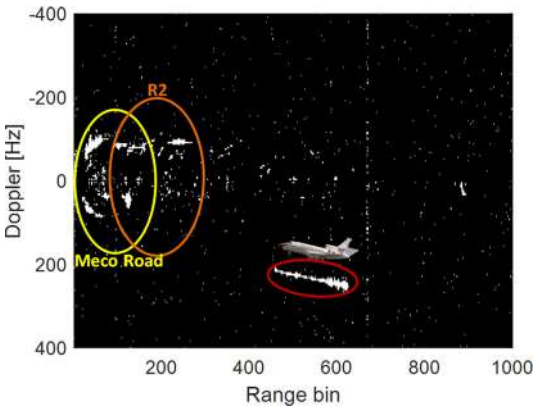

Fig. 26. Superposition of the 80 CFAR detection matrices generated throughout all the acquisition time.

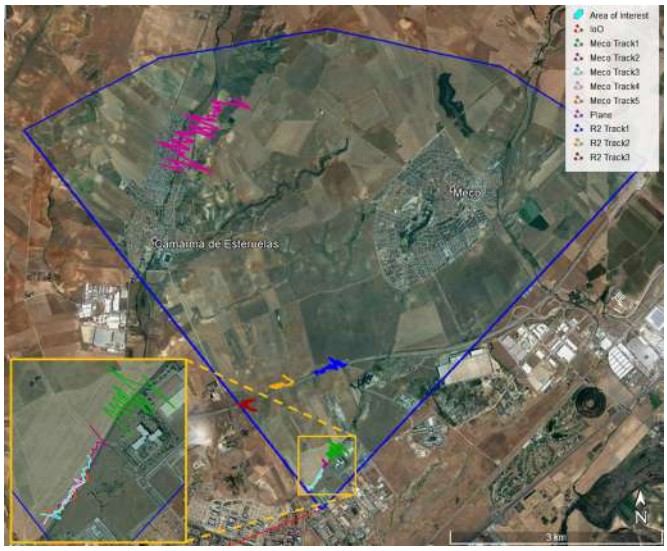

Fig. 27. Targets' trajectories generated after DoA estimation through array processing techniques.

tenna requirements were defined for the specific PR surveillance application. Bandwidth and radiation pattern requirements were challenging because of the use of UHF frequencies, which are lower than typical radar ones. An antenna prototype was manufactured and characterized in an anechoic chamber, proving the fulfilment of all the defined requirements.

A circle shaped patch antenna was selected as starting point. The basic design was improved employing aperture coupled feeding with thick air substrate, and a novel boxed reflector that achieved a wider azimuth beamwidth. H-shaped aperture was proposed for the coupled feeding, and some modifications in the patch, as adding top substrate and modifying the fundamental shape with and optimized slot. Measurements in anechoic chamber showed a wide impedance bandwidth of 31.8%, gain of 6.5 dBi, and azimuth and elevation beamwidths of 90° and 70°, respectively.

Taking into consideration that the new version of the IDEPAR demonstrator allowed the acquisition of 12 consecutive DVB-T channels, and the availability of eight acquisition chains, a NULA of 7 elements was designed, manufactured and validated, preserving the eighth channel for the acquisition of the reference signal. A design method based on that presented in [12] was proposed, that transformed the experimental factor defined to control the main beamwidth in a new optimization variable, and included coupling effects, controlling the associated computational cost.

A comparative study was performed considering other single radiating elements and array architectures described in the literature. Results proved the interest in the design of array antennas in UHF, and the relevance of the defined design requirements. Research contributions in this field are expected to be applied to face design requirements defined by 5G communication services that will operate in the 800 MHz band.

The manufactured NULA was integrated in IDEPAR demonstrator and validated with radar measurements in the defined radar scenario.

Declaration of competing interest

The authors declare that they have no known competing financial interests or personal relationships that could have appeared to influence the work reported in this paper.

References

[1] IEEE Standard Radar Definitions, IEEE Aerospace and Electronic Systems Society, Std 686, 2008.

[2] N.J. Willis, Bistatic Radar, Scitech Publishing Inc., 2005.

[3] P.E. Howland, D. Makisimiut, G. Reitsma, FM radio based bistatic radar, IEE Proc. Radar Sonar Navig. 152 (3) (2005), https://doi.org/10.1049/ip-rsn:20045077.

[4] M. Malanowski, et al., Experimental results of the PaRaDe passive radar field trials, in: 2012 13th International Radar Symposium, Warsaw, 2012, pp. 65–68.

[5] H. Kuschel, J. Heckenbach, S. Muller, R. Appel, On the potentials of passive, multistatic, low frequency radars to counter stealth and detect low flying targets, in: 2008 IEEE Radar Conference, Rome, 2008, pp. 1–6.

[6] M.P. Jarabo-Amores, D. Mata-Moya, P.J. Gomez-del-Hoyo, J.L. Barcena-Humanes, J. Rosado-Sanz, Drone detection feasibility with passive radars, in: 15th European Radar Conference, Madrid, 2018, pp. 313–316.

[7] N. del Rey-Maestre, D. Mata-Moya, M.P. Jarabo-Amores, P.J. Gomez-DelHoyo, J. Rosado-Sanz, Optimum beamforming to improve UAV's detection using DVB-T passive radars, in: Accepted in International Radar Conference, Toulon, 2019.

[8] M. Malanowski, K. Kulpa, Digital beamforming for passive coherent location radar, in: IEEE Radar Conference, 2008.

[9] R. Mueller, R. Lorch, Broadband biquad UHF antenna array for DOA, in: 2015 9th European Conference on Antennas and Propagation (EuCAP), Lisbon, 2015, pp. 1–5.

[10] A. Capria, et al., Multifunction imaging passive radar for harbour protection and navigation safety, IEEE Aerosp. Electron. Syst. Mag. 32 (2) (February 2017) 30–38, https://doi.org/10.1109/MAES.2017.160025.

[11] G. Bournaka, J. Heckenbach, A. Baruzzi, D. Cristallini, H. Kuschel, A two stage beamforming approach for low complexity CFAR detection and localization for passive radar, in: 2016 IEEE Radar Conference, 2016.

[12] N. del Rey-Maestre, D. Mata-Moya, M.P. Jarabo-Amores, P.J. Gomez-DelHoyo, J.L. Barcena-Humanes, J. Rosado-Sanz, Passive radar array processing with non-uniform linear arrays for ground target's detection and localization, Remote Sens. (2017), https://doi.org/10.3390/rs907075.

[13] D.W. O'Hagan, M. Schroder, V. Basavarajappa, P. Knott, H. Kuschel, M. Simeoni, Wideband antenna array for digital video broadcast terrestrial-based passive bistatic radar applications, IET Radar Sonar Navig. 8 (2) (February 2014) 106–113, https://doi.org/10.1049/iet-rsn.2013.0182.

[14] M. Conti, C. Moscardini, A. Capria, SMARP passive radar for harbour protection and navigation safety: trials results, in: International Conference on Radar Systems (Radar 2017), Belfast, 2017, pp. 1–6.

[15] R. Saini, M. Cherniakov, DTV signal ambiguity function analysis for radar application, IEE Proc. Radar Sonar Navig. 152 (3) (2005), https://doi.org/10.1049/ip-rsn:20045067.

[16] J.E. Palmer, H.A. Harms, S.J. Searle, L. Davis, DVB-T passive radar signal processing, IEEE Trans. Signal Process. 61 (8) (April 2013) 2116–2126, https://doi.org/10.1109/TSP.2012.2236324.

[17] M.P. Jarabo-Amores, J.L. Bárcena-Humanes, P.J. Gómez-del-Hoyo, N. Rey-Maestre, D. Juara-Casero, F.J. Gaitán-Cabañas, D. Mata-Moya David, IDEPAR: a multichannel digital video broadcasting-terrestrial passive radar technological demonstrator in terrestrial radar scenarios, IET Radar Sonar Navig. 11 (1) (2017) 133–141, https://doi.org/10.1049/iet-rsn.2016.0087.

[18] J.L. Barcena-Humanes, J. Martin-de-Nicolas, C. Solis-Carpintero, M.P. Jarabo-Amores, M. Rosa-Zurera, D. Mata-Moya, DVB-T ambiguity peaks reduction in passive radar applications based on signal reconstruction, in: European Radar Conference (EuRAD), 2014.

[19] Digital Video Broadcasting (DVB): Framing Structure, Channel Coding and Modulation for Digital Terrestrial Television DVB-T, European Telecommunication Standards Institute, 2004.

[20] K. Park, D. Lee, J. Seo, Dual-polarized GPS antenna array algorithm to adaptively mitigate a large number of interference signals, Aerosp. Sci. Technol. 78 (2018) 387–396, https://doi.org/10.1016/j.ast.2018.04.029.

[21] J. Appel, Adaptive space-time process in radar applications, Aerosp. Sci. Technol. 1 (2) (1997), https://doi.org/10.1016/S1270-9638(97)90044-4, 151-161-396.

[22] L. Gong, M. Yu, A new Gaussian mixture method with exactly exploiting the negative information for GMTI radar tracking in a low-observable environment, Aerosp. Sci. Technol. 80 (2018) 1–10, https://doi.org/10.1016/j.ast.2018.06.030.

[23] A. Gómez-Rodríguez, A. Sánchez-Carmona, L. García-Hernández, C. Cuerno-Rejado, Remotely piloted aircraft systems conceptual design methodology based on factor analysis, Aerosp. Sci. Technol. 90 (2019) 368–387, https://doi.org/10.1016/j.ast.2019.04.041.

[24] G. Zhang, L. Hsu, Intelligent GNSS/INS integrated navigation system for a commercial UAV flight control system, Aerosp. Sci. Technol. 80 (2018) 368–380, https://doi.org/10.1016/j.ast.2018.07.026.

[25] B.T.P. Madhav, et al., Circular array antenna synthesis based on element spacing, Int. J. Appl. Eng. Res. 9 (20) (Sep 2014) 6959–6965.

[26] N. del-Rey-Maestre, M. Jarabo-Amores, D. Mata-Moya, J. Bárcena-Humanes, P.G. del Hoyo, Machine learning techniques for coherent CFAR detection based on statistical modeling of UHF passive ground clutter, IEEE J. Sel. Top. Signal Process. 12 (1) (Feb. 2018) 104–118, https://doi.org/10.1109/JSTSP.2017.2780798.

[27] J. Rosado-Sanz, N. Rey-Maestre, D. Mata-Moya, M.P. Jarabo-Amores, M. Rosa-Zurera, J.L. Barcena-Humanes, Advantages of non-uniform linear arrays based on COTS elements in passive radar applications, in: 2018 22nd International Microwave and Radar Conference (MIKON), Poznan, Poland, 2018.

[28] C.A. Balanis, Antenna Theory: Analysis and Design, John Wiley & Sons Inc., 2016.

[29] M.V.T. Heckler, A. Dreher, Performance of microstrip antenna arrays installed on aircraft, Aerosp. Sci. Technol. 26 (1) (2017) 235–243, https://doi.org/10.1016/j.ast.2012.05.002.

[30] A. Boufrioua, A. Benghalia, Effects of the resistive patch and the uniaxial anisotropic substrate on the resonant frequency and the scattering radar cross section of a rectangular microstrip antenna, Aerosp. Sci. Technol. 10 (3) (2006) 217–221, https://doi.org/10.1016/j.ast.2005.11.010.

[31] G. Kumar, K.P. Ray, Broadband Microstrip Antennas, Artech House Inc., 2003.

[32] L. Zaid, G. Kossiavas, J.Y. Dauvignac, A. Papiernik, Very compact double C-patch antenna, Electron. Lett. 34 (10) (14 May 1998) 933–934, https://doi.org/10.1049/el:19980710.

[33] B.-K. Ang, B.-K. Chung, A wideband E-shaped microstrip patch antenna for 5 - 6 GHz wireless communications, Prog. Electromagn. Res. 75 (2007) 397–407, https://doi.org/10.2528/PIER07061909.

[34] M.T. Islam, M.N. Shakib, N. Misran, Broadband E-H shaped microstrip patch antenna for wireless systems, Prog. Electromagn. Res. 98 (2009) 163–173, https://doi.org/10.2528/PIER09082302.

[35] M.L.S.N.S. Lakshmi, H. Khan, B.T.P. Madhav, Novel sequential rotated 2 × 2 array notched circular patch antenna, J. Eng. Sci. Technol. Rev. (ISSN 1791-2377) 8 (4) (Dec. 2015) 73–77.

[36] J. Rosado-Sanz, M.P. Jarabo-Amores, D. Mata-Moya, N. Rey-Maestre, P. Gomez-del-Hoyo, Design of a broadband patch antenna for a DVB-T based passive radar antenna array, in: IEEE International Conference on Ubiquitous Wireless Broadband, Salamanca, Spain, 2017.

[37] J. Rosado-Sanz, M.P. Jarabo-Amores, D. Mata-Moya, N. Rey-Maestre, J.L. Barcena-Humanes, SLL optimization of passive radar non-uniform linear arrays based on commercial UHF antennas, in: International Conference on Control, Artificial Intelligence, Robotics and Optimization (ICCAIRO), Prague, Czech Republic, 2017.

[38] Harry L. van Trees, Optimum Array Processing: Part IV of Detection, Estimation, and Modulation Theory, Wiley-Interscience, 2002.

[39] R.B. Lewis, V. Torczon, Pattern Search Methods for Linearly Constrained Minimization, Institute for Computer Applications in Science and Engineering NASA, Virginia, EEUU, 1998.

[40] F. Colone, D.W. O'Hagan, P. Lombardo, C.J. Baker, A multistage processing algorithm for disturbance removal and target detection in passive bistatic radar, IEEE Trans. Aerosp. Electron. Syst. 45 (2) (2009) 698–722, https://doi.org/10.1109/TAES.2009.5089551.